Proceedings of ASME Turbo Expo 2013
TE 2013
June 3-7, 2013, San Antonio, Texas, USA

DRAFT GT2013-95461

VALIDATION OF FLOW FIELD AND HEAT TRANSFER IN A TWO-PASS INTERNAL COOLING CHANNEL USING DIFFERENT TURBULENCE MODELS

Federica Farisco, Stefan Rochhausen*, Metin Korkmaz, Michael Schroll
Institute of Propuslion Technology
German Aerospace Center (DLR)
Cologne, Germany
Email: federica.farisco@gmail.com

ABSTRACT

In this work the flow regime within a generic turbine cooling system is investigated numerically. The main objective is to validate the performance of various turbulence models with different complexity by comparing the numerical results with experimental data. To maximize surface heat transfer rates, present-day cooling systems of high pressure turbines have highly complex shapes generating high turbulence levels and flow separations. These flow structures lead to higher requirements of CFD-techniques for sufficient prediction. To simulate complex flows in the industrial design process, Reynolds averaged Navier-Stokes (RANS) techniques are applied instead of computationally expensive LES and DNS simulations. Therefore, higher order turbulence models are necessary to predict flow field and heat transfer performance in such complex motion. The DLR standard flow solver for turbomachinery flows, TRACE, is used to solve the RANS equations. Four turbulence models have been analysed: the one equation model of Spalart and Allmaras, the two equation $k-\omega$ model of Wilcox, the two equation $k-\omega$ SST model of Menter and the anisotropy resolving Explicit Algebraic Reynolds Stress model (EARSM) of Hellsten. The investigated cooling geometry consists of a two-pass smooth channel with a 180 degree bend. At the DLR institute of propulsion technology PIV measurements in a rotating cooling channel test bed for Rotation numbers up to 0.1 have been performed. This work uses the experimental data for Re=50,000 and Ro=0 without rotation for comparison. For all models adiabatic and diabatic calculations have been performed. In order to accurately apply the turbulence models, a study concerning the turbulent boundary conditions has been performed prior to the calculations. The results obtained through RANS simulations are presented in comparison with the experiments along planes in the flow direction and in the orthogonal direction to study the velocity field, the shape and size of the separation bubbles and the wall shear stress. The EARSM predicts the flow field overall more accurately with improved agreement between all relevant parameters compared to the other models. The diabatic simulations reflect the adiabatic results. However, it can be noticed that higher complexity in turbulence modelling is related to increased heat transfer. Our work confirms the EARSMs ability to predict complex flow structures better than the more elementary approaches.

*Address all correspondence to this author.

NOMENCLATURE

Re	Reynolds Number	
Ro	Rotation Number	
St	Stanton Number	
C_f	Friction Factor	
P_{T1}	Total Pressure Inlet	$[bar]$
P_{T2}	Total Pressure Outlet	$[bar]$
P_2	Static Pressure Outlet	$[bar]$
Pr_t	Turbulent Prandtl Number	
c_∞	Velocity	$[m/s]$
c_p	Specific Heat	$[J/(KgK)]$
X	Streamwise Direction	
Y	Wall-normal Direction	
Z	Spanwise Direction	
α	Heat Transfer Coefficient	$[W/(m^2K)]$
ρ_∞	Density	
τ_w	Shear stress wall	
LES	Large Eddy Simulation	
DNS	Direct Numerical Simulation	
DES	Detached Eddy Simulation	
DLR	German Aerospace Center	
PIV	Particle Image Velocimetry	
TKE	Turbulent Kinetic Energy	
HTC	Heat Transfer Coefficient	
RAF	Reynolds Analogy Factor	

INTRODUCTION

Designing cooling systems for high pressure turbines is a challenging task that tries to compromise two main requirements: Reducing the demand of highly pressurised cooling air and simultaneously reducing turbine surface temperatures in hot gas flow regimes. This task requires a detailed understanding of the aero-thermal-phenomena in the turbine. For example in the turbine internal cooling channel the coolant flows through a multi-passage circuit from hub to tip. Typically these passages are connected by 180 degree bends to change the flow direction from radially inward to radially outward. From a computational point of view the turning of the flow is a complicated task. Turning the flow gives rise to anisotropic flow structures such as Dean vortices and furthermore causes the flow to separate from the surface.

In the literature a large amount of studies can be found on experimental and numerical investigation of turbine cooling. Review papers by [1, 2, 3] provide an overview of recent progress. Similar cooling channel geometries have been investigated by several reserchers [4, 5, 6] coming to the conclusion that $k\omega$-SST performs best in such flows and presents its superiority against other two equation modelling approaches.

Studies by [7] compared two equation models with higher order turbulence closures (RSM) and LES. As expected these methods were able to make more accurate predictions while the computational time increased significantly. In industrial design process it would be desirable use accurate RANS flow simulations that are able to capture the dominant flow features and benefit from the low computational time compared to LES or DES methods.

The aim of the current paper is to study the ability of the RANS code TRACE, which has been mostly used for the design of multistage transonic compressors and turbines, to model turbine internal cooling flow. Four different turbulence models - the one-equation Spallart-Almaras Model, two kω-models of Wilcox and Menter as well as the anisotropic explicit algebraic reynolds stress modell of [8] - have been investigated to rank their ability to predict the complex flow field of an U-bend cooling channel with non-parallel walls. These simulations have been compared to PIV measurements have been made by [9].

Furthermore diabatic calculations have been carried out for all four turbulence models which provide a database for future comparisons with experimental heat transfer data. Comparisons have been analysed between HTC and velocity flow field results pointing out and confirming their existing links.

Numerical Method

All simulations presented in this paper have been carried out with the TRACE-code. [10] TRACE, which is developed at DLRs Institute of Propulsion Technology, is established as the DLRs standard code for internal and turbomachinery flows. In its default configuration TRACE solves the Reynolds averaged Navier-Stokes equations in the finite volume formulation on multi-block curvilinear meshes. Convective fluxes of the RANS equations are discretized by the TVD upwind scheme by Roe, for viscous fluxes central differences are used. An implicit numerical scheme is used for more stable and rapid convergence [11].

For modelling turbulence in TRACE several models of different complexity are available in TRACE. The one-equation model of Spalart and Allmaras [12] is simplest approach used in this paper. Furthermore two different two-equations models, the Wilcox-k-w-model [13] and the Menter-SST model [14] have been used. The fourth model used in this report is the anisotripoc explicit algebraic model of Hellsten [8]. The turbulence modelling approach of Hellsten is formulated on the two equation $k\omega$-basis and takes into account an extra anisotropy.

PIV measurements

The complete flow maps of the instantaneous as well as averaged flow field inside the cooling channel where obtained with two-component Particle Image Velocimetry (2C PIV), working even at high turbulence levels, which are typical for the narrow serpentine-shaped cooling systems [16, 15]. PIV is a non-intrusive optical planar measuring technique based on the principle of measuring the displacement of small tracer particles

(aerosol, diameter < 1 μm) within the investigated flow field. Two laser flashes, each with a flash duration of only few nanoseconds, are formed into a light sheet of about 1 mm thickness and illuminate the flow field twice within a few microseconds. The light scattered by the tracer particles is recorded via a CCD camera and enables the simultaneous acquisition of two component velocity data over the illuminated area [17,18]. The flow following behaviour of the tracer particles even at strong centrifugal forces like in this test case is assured if they have a mean diameter < 1 μm. The used aerosol generator provides oil droplets of about 0.8 μm. Laser illumination is provided by a standard, frequency-doubled, dual cavity Nd:YAG laser with 50 mJ pulse energy at 532 nm (green) and maximum repetition rate of 15 Hz (Quantel CFR Brio 50) and guided via a light sheet optic to the desired measuring plane within the flow with a mean thickness of about 0.8 mm. On the recording side, thermo-electrically cooled, interline-transfer CCD cameras (pco.2000, 2048 $\times$ 2048 pixel, pixel size 7.4 $\times$ 7.4 μm^2, 14 bit, 7 fps, 4 GB camRAM) are used with macro lenses (Zeiss 85 and 100 mm) and band pass filters in front. With a centre frequency of 532 nm and 5 nm bandwidth (FWHM) the filter reject most of the unwanted background light. The reached magnification factors are between 16.5 pixel/mm for the main flow field in the radial orientated planes [15] and 47.3 pixel/mm for the secondary flow field in the axial cross planes [16]. To obtain velocity maps the collected image pairs were processed with the PIV software PIVview2C which implants a state-of-the-art multi-grid interrogation algorithm with an initial sampling window of 96 $\times$ 96 pixel and final window size of 24 $\times$ 24 pixel on a sampling grid of 12 $\times$ 12 pixel. The velocity vector maps are averaged out of about 900 images for main flow field and 1,500 images for secondary flow field. The accuracy of the PIV measurements technique itself for the non-rotating model is better than 1% of full scale. This is confirmed both by means of reference measurements performed on a calibration nozzle as well as by comparison with Laser Two Focus (L2F) velocimetry measurements in the same model [19]. Following the approach made by Westerweel [20] the estimated measurement error made at optimal PIV measurements conditions is in the order of 0.1 pixels resulting in a relative measurement error of 0.42 and 0.8 m/s in the absolute domain.

Mesh Independency Study

In order to ensure mesh independency a mesh study of the two-pass internal cooling channel has been performed starting from an original mesh used by DLR [21]. Hereby the main focus has been the wall normal resolution of the mesh in the cooling channel.

The first cell-center of the coarsest mesh is located at an average non-dimensional wall distance of $y^+ \approx 1$. The coarsest mesh has been refined successively by using the half cell height in both directions orthogonal to the flow. By reducing the wall distance to one half, the wall normal resolution has been refined in four steps. Details of average cell distance and overall number of mesh cells are shown in Tab. 1.

Name	y^+	Mesh Cells (in Mio.)	Rel. Loss Coeff.
Mesh A	1 - 2	≈ 0.6	+29%
Mesh B	0.5 - 1	≈ 2.2	+4%
Mesh C	0.2 - 0.4	≈ 8.4	-0.99%
Mesh D	0.1 - 0.2	≈ 32	0%

TABLE 1. MESH STUDY

All four meshes have been used for calculations with Wilcox $k\omega$ turbulence modelling. To rank the influence of the different mesh resolutions a global parameter, the loss coefficient, has been analysed. The loss coefficient for each mesh have been calculated by the equation (1)

$$\zeta = \frac{P_{T1} - P_{T2}}{P_{T2} - P_2} \tag{1}$$

The loss coefficient, which has been calculated for the finest mesh, has been defined to be the reference value. All other values have been non-dimensionalised with this reference to show the relative error. Table 1 shows the loss coefficient relative error related to the mesh numbers of nodes. It can be observed that a relatively low error could be obtained with mesh C. This mesh has been chosen, since it ensures a good balance between the lowest error in terms of losses and less computational time steps compared with the others.

In this short mesh dependency study it has been shown that the classical low Reynolds approach ($y^+ \approx 1$) is not accurate enough for this configuration. An overall loss that is not significantly affected by the mesh requires a mesh below $y^+ \approx 0.5$.

Turbulence Model Boundary Conditions Set

Modelling turbulence with transport equations requires specification of the turbulent boundary conditions. Prior to comparing different turbulence models a study has been done to determine these boundary conditions. The PIV measurements provide a valuable source for the turbulent motion of the flow. From measured data it was possible to calculate the turbulent kinetic energy in the leading edge channel that can be used to define numerical boundary conditions.

However in this study it has been found that due to the shape of the plenum strong vortical structures occur. Turbulence kinetic energy production meachanisms in the plenum dominate. In figure 1 the TKE production caused by the plenum is shown. The

vortex structures along the plenum walls and corners have been visualised. In the investigated geometry no significant influence of the inlet turbulent boundary conditions has been found on the TKE in the leading edge channel.

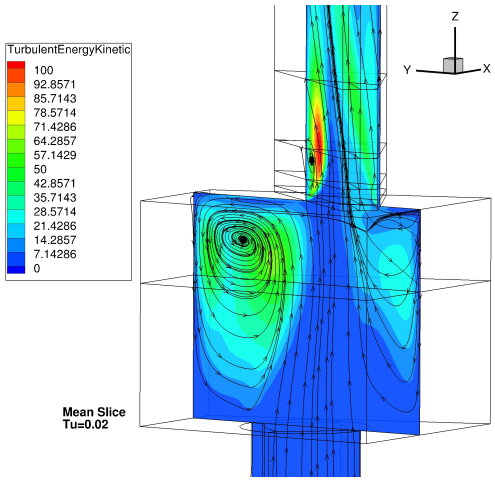

FIGURE 1. TKE PLENUM EXAMPLE

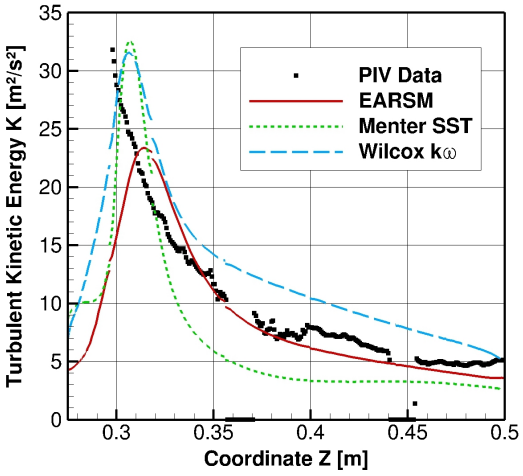

FIGURE 2. TKE TURBULENCE MODELS COMPARISONS

In figure 2 the numerical results of TKE obtained along the plenum outlet and the leading edge duct have been compared to experimental data. Close to the plenum/channel interface, where turbulence production reaches its maximum value, all turbulence models show high values of TKE. Wilcox-$k\omega$ and Menter-SST successfully predict the maximum TKE value at z = 0.3 in agreement with the experimental data. Differences between numerical data and experiments can be observed in the decay rates along the channel. The EARSM turbulence model fails in predicting the maximum TKE value, but simulates a decay rate along the channel according to the PIV data. At the end of the leading edge channel at z = 0.5 the differences between the numerical results and PIV data become small compared to the experimental uncertainty.

Adiabatic Steady RANS Simulations

Following the discussion in the previous sections for the turbulence model comparison the refined mesh C has been chosen. In this section the numerical flow field validation is discussed for steady simulations with adiabatic walls. Through experimental PIV measurements the numerical flow solutions have been verified. Due to the 180 degree bend a massive flow separation occurs in the flow field. Such large flow simulations are challenging for steady RANS simulations. Calculations have been considered as converged when the L1-averaged residual was below 10^{-6}. For all large scale structures in the flow field no further variation has been observed with further timesteps.

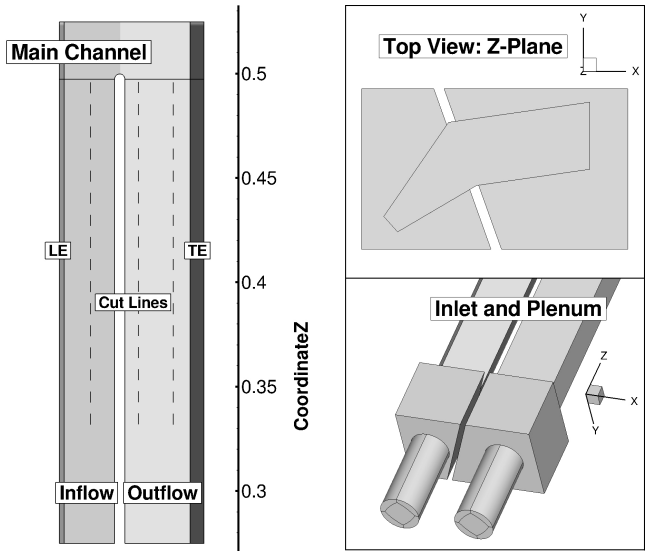

FIGURE 3. GEOMETRY OVERVIEW B

The experimental dataset is distributed along planes in streamwise (Z direction as shown in figure 3) and orthogonal direction to the main flow along the Z-Plane (figure 3).To compare numerical and PIV data, the CFD results have been evaluated through these planes. Furthermore the parameters along the cutting lines have been considered to compare predictions of main flow velocity (figure 3). As second step planes at constant Z-coordinate have been analysed, pointing out vortical secondary structures of the flow.

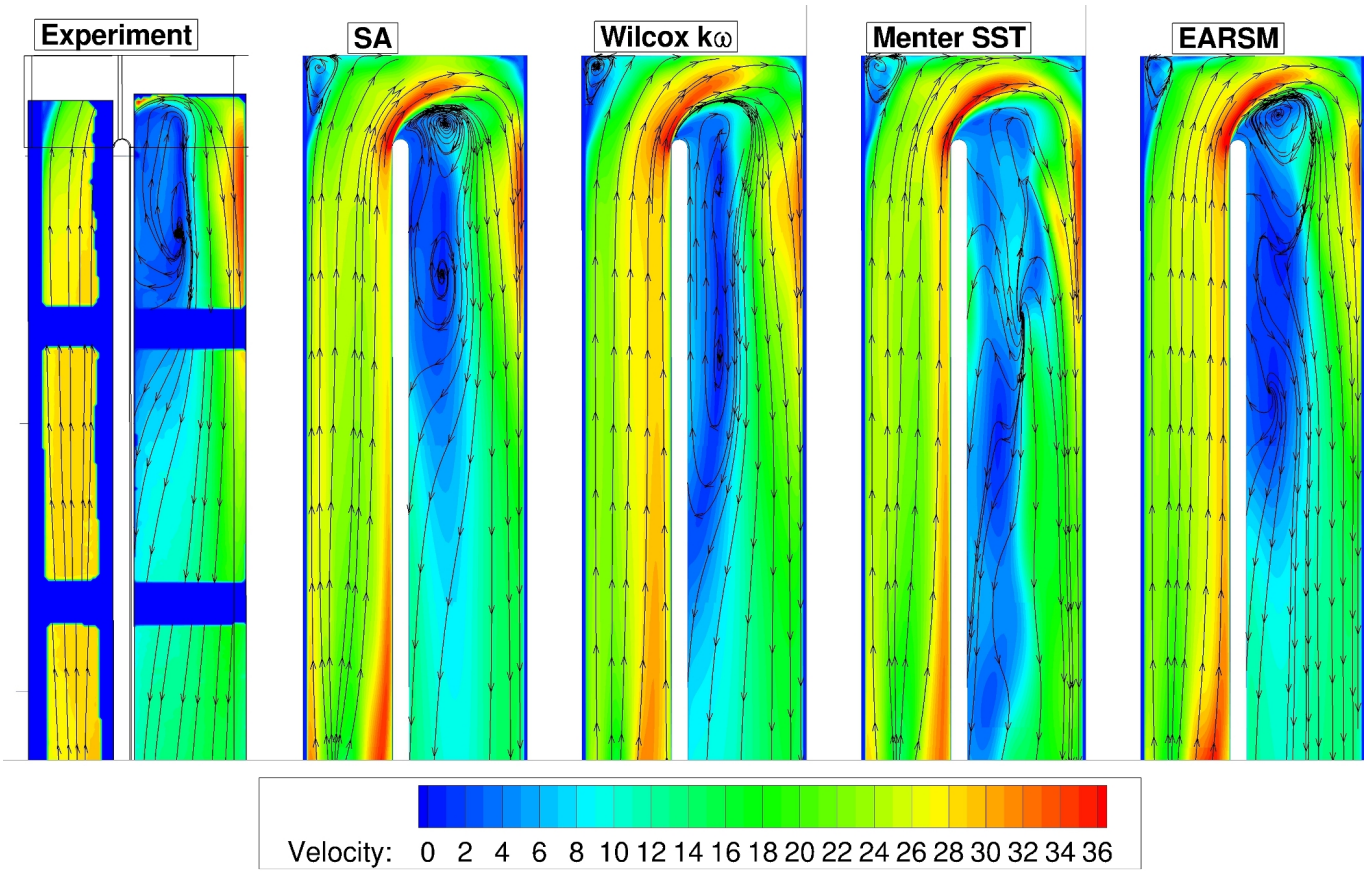

FIGURE 4. VELOCITY MEAN LINE COMPARISONS

Primary Velocity 2D Analysis

In figure 4 the absolute velocity 2D behaviour is presented for all turbulence models compared to experimental data. In the PIV data the velocity profile is quite homogenous upstream of the bend. In contrast all simulations predict low velocities in the middle of the channel and higher values at the edges. Before entering the bend, the flow accelerates near the inner wall and decelerates along the outer wall generating a “dead“ region of lower values which is evident in all models. At the beginning of the T.E. duct the flow accelerates near the outer wall and decelerates along the inner region. In this zone downstream of the bend a large separation bubble develops, caused by the inability of the flow to follow the turn. The bubble shows different shapes and lengths for the various models. The recirculation region size predicted by the SA model resembles the PIV measurements. In contrast to the PIV measurements where a single large vortex occurs, two counter rotating vortices are visible in the SA model. The Wilcox model successfully predicts the vortex structure but the backflow region size is too large. EARSM and Menter SST deviate in size and vortex structure. Along the T.E. duct moving towards the outlet, the influence of the bend decreases and the homogenous velocity profile gradually redevelops. The lowest velocities are concentrated in the recirculation regions, where the vortex lines forming loops, for all turbulence models and the experiment. Quantitative velocity comparisons between numerical models and experimental data are presented in the graphics in figure 5, 6 and 7. The first diagram (figure 5) presents the velocity levels along a mean line with which the leading edge duct has been cut. The positions of the cutting lines are provided in figure 3. As previously discussed, the shape of the plenum is responsible for the development of strong vortices which in turn cause the peak in the values in the inlet. Compared to experiment the best trend is predicted by the models of Wilcox k-ω and EARSM. The diagram in figure 6 shows the velocity values along the mean slice of the first half of the trailing edge channel in the inner region where the separation bubble develops. At the beginning of the T.E. duct the velocity changes its direction reaching the lowest negative values where the separation bubble occurs. After the reattachment point the velocity levels increase to positive values achieving the highest values for the SA and EARSM models that present the most similar trend compared to experiments. The third diagram (figure 7) presents the velocity

levels along the mean slice of the second half of the trailing edge duct in the outer region where the Dean vortices occur. Along the bend region all models reach the highest velocity values due to the blockage of the backflow that accelerates the fluid. In this area SA and EARSM show similar behaviour to PIV data. Along the core region of the duct until the exit of the channel EARSM presents the lowest levels and Wilcox $k\omega$ fits in a more accurate way the experiments. SST model distinguishes itself from the others presenting the most evident fluctuating behaviour along the entire duct.

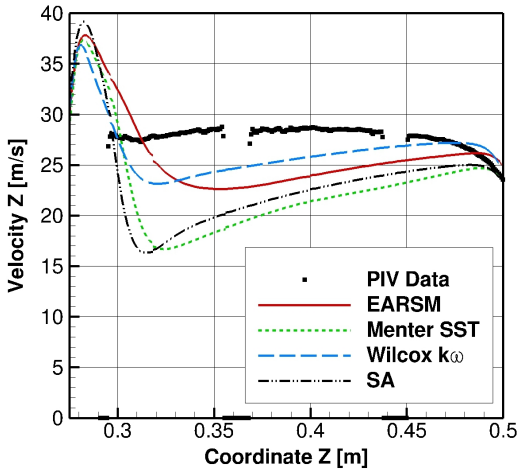

FIGURE 5. VELOCITY L.E. DIAGRAM COMPARISONS

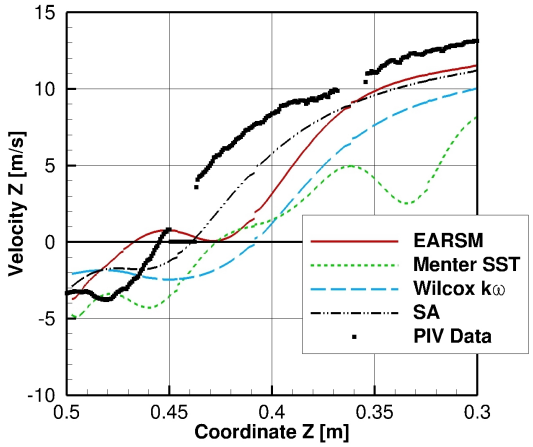

FIGURE 6. VELOCITY T.E. INNER

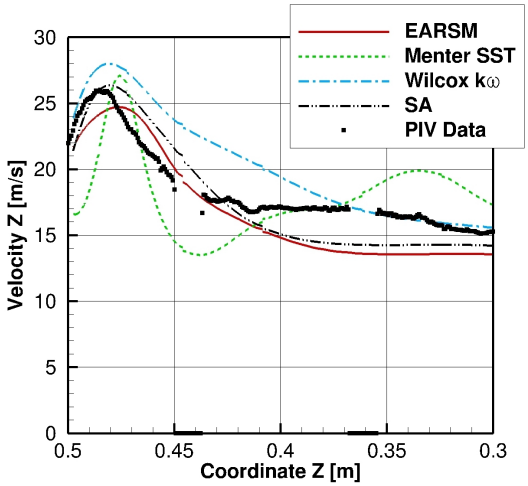

FIGURE 7. VELOCITY T.E. OUTER

Separation and Reattachment Phenomena

One of the areas of great interest is the bend region where occurs the separation bubble.

Observing the Tab.2 the different quantitative bubble lengths can be analysed. Spalart Allmaras and EARSM are the turbulence models that present the nearest bubble lengths compared to experiments. The bubble shape in SA model is the most similar to PIV data. This confirms the SA trend analysed in figure 7 where the turbulence model presented the nearest behaviour to experimental data along the bend region. EARSM model shows the major bubble thickness that is the most similar to PIV data. This observation could explain the EARSM trend analysed in figure 7 where the model presents the lowest velocity levels. Menter SST shows a different bubble shape compared to the other models and its behaviour could be linked to the fluctuations observed in figure 7 along the most part of the trailing edge channel.

	Reattachment point	Bubble length
Exp Data	0.455	0.045
SA	0.44	0.06
Wilcox k-ω	0.41	0.09
SST	0.425	0.075
EARSM	0.433	0.067

TABLE 2. SEPARATION BUBBLE LENGTHS

Secondary Velocities 2D Analysis

The secondary flow in three planes orthogonal to the main direction has been analysed in figure 8.

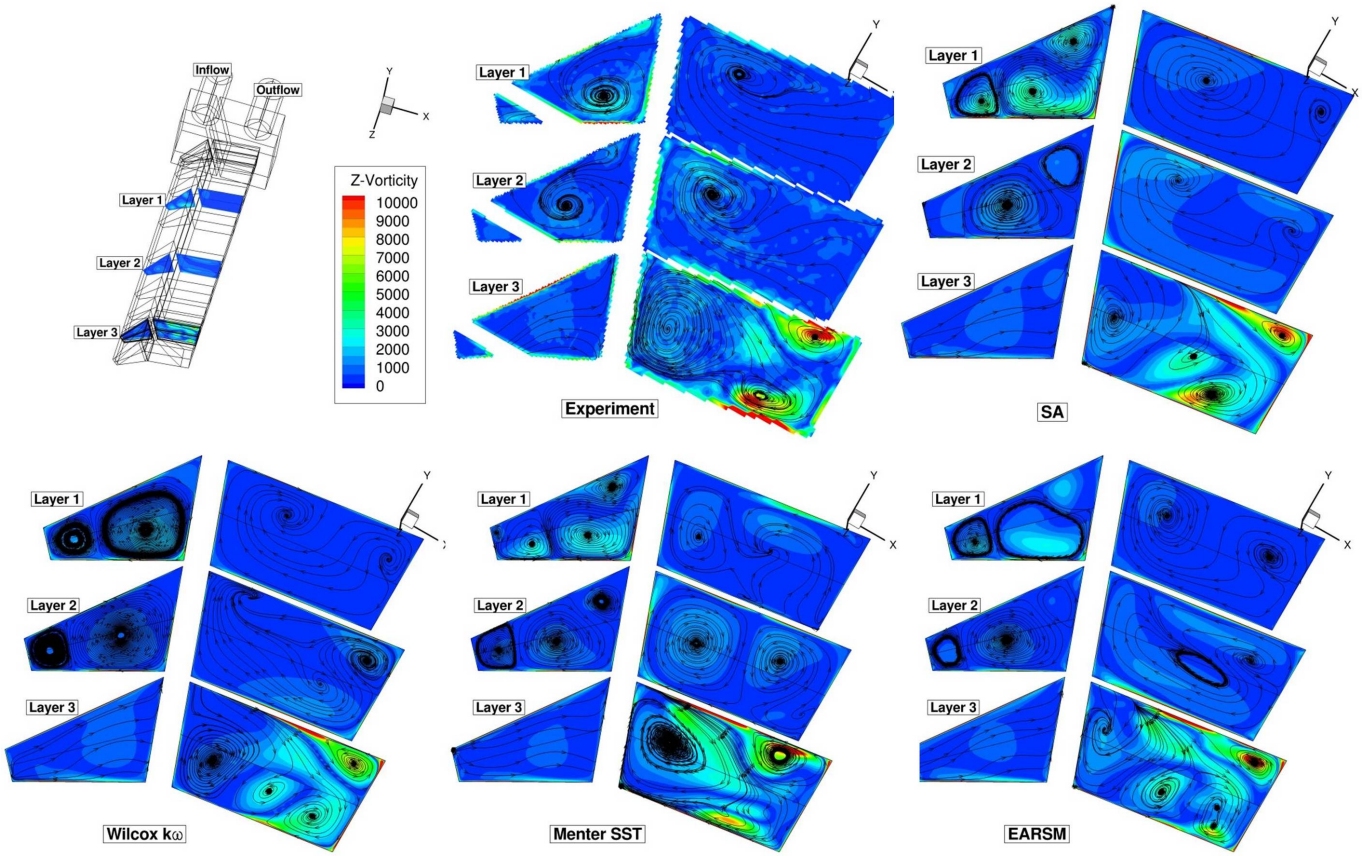

FIGURE 8. GLOBAL OVERVIEW VORTICITY

This 3D layout gives a global overview of the vortex development along the geometry. First the Layer 3 should be discussed. This plane is the nearest to the bend crossing the separation bubble and showing clearly the development of the principal secondary vortical structures. The biggest vortical structure that occurs in experiments along the inner sidewall is due to the part of the flow directed to the exit of the duct. This flow separates at the corner of the bend generating a big clockwise vortex that brings fluid from the surface to the middle of the duct. In all turbulence models this vortical structure is replaced with several smaller vortices. The most similar behaviour to experiments is reached by SST that shows along the inner sidewall the widest vortex compared with the other models. The part of the flow that hits the outer sidewall generates along the corners two counter-rotating vortices (Dean vortices). They are induced by the pressure gradient between the inner and outer surface. These vortices lead the fluid from the core towards the outer regions, bringing to much higher velocity values [21, 22, 23]. Comparing the different Layers it can be concluded: all turbulence models present three vortices along the leading edge duct. All models distinguish themselves from the experiments in the leading edge channel. The PIV data show just a big vortex even if in the region where the data are not available a vortical structure could be developed. Along the trailing edge duct starting from the third layer to the first one, the vorticity levels decay quickly. It can be observed that the highest measured values in the core of the Dean vortices have not been simulated by the turbulence models. To summarise it can be stated: the overall performance in predicting accuracy of the four turbulence models investigated differs a lot. Three models SA, Wilcox $k\omega$ and EARSM give reasonable predictions concerning absolute values of streamwise velocity. The Menter SST model is able to predict the secondary flow structure to a certain degree.

Diabatic Steady RANS Simulations

Heat Transfer Analysis

All calculations that have been presented so far have been adiabatic calculations. However in turbine cooling channel design, the ability of the flow of transfering heat is of central interest. In this section calculations with an increased surface temperature will be presented ($T_{wRef} = 310K$). In order to keep buoyancy effects a small temperature difference ΔT=10K has been chosen. HTC has been calculated by the equation 2.

$$HTC = \frac{HeatFluxWall}{Temperature - T_{wRef}} \tag{2}$$

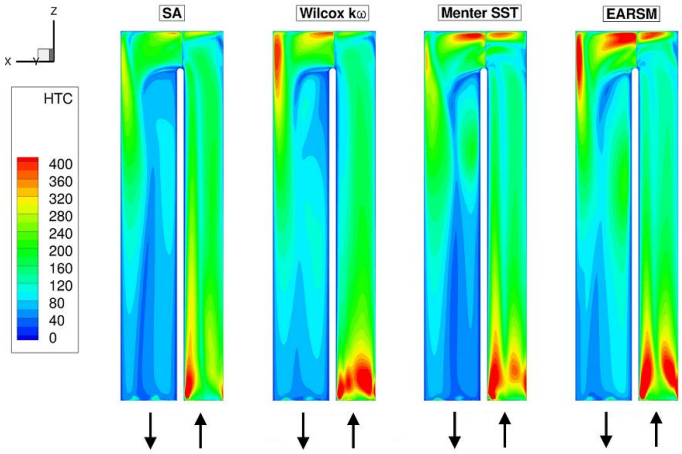

FIGURE 9. HTC SUCTION SIDE WALL

In figure 9 HTC is evaluated for each turbulence model along the suction side wall of the geometry. All models predict a similar trend: moderate values before the bend near the inner region, much higher levels along the outer surface of the bend and the outer sidewall of the T.E. duct. The peak values occur in a progressively wider region proceeding from SA, Wilcox until SST and EARSM. A much higher complexity in turbulence modelling leads to an increase in HTC. The highest order model EARSM leads to a major extension of the regions with higher heat transfer. Experimental studies have shown that the reattachment process in separated flows is accompanied by a substantial increase of heat transfer coefficient compared to an attached boundary layer [24].

This trend is reversed in the T.E. duct where deceleration takes place along the inner wall while acceleration occurs near the outer wall leading in this zone to much higher HTC values. The pressure gradient between the inner and outer surfaces causes the development of two counter-rotating vortices. These vortical structures bring fluid from the core to the outer wall, resulting in a higher heat transfer coefficient along the outer wall and confirming the velocity profiles discussed in the section before. The separation bubble that occurs near the inner surface downstream of the bend, brings the vortices towards the outer wall. They disappear gradually along the T.E. duct.
Along the inlet duct before the bend the HTC profile present a behaviour on the average flatter.

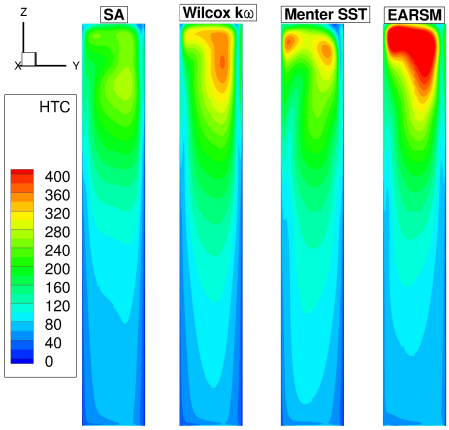

FIGURE 10. HTC OUTER SIDEWALL

In figure 10 the HTC trend for each model is analysed along the outer sidewall of the channel. Through the study of this plane the highest values reached by HTC can be clearly observed confirming the Wall Shear Stress behavior studied in the velocity flow field analysis. The highest HTC values are in agreement with the highest levels of wall shear stress and they are reached in the regions where the vortices hit the wall presenting their maximum force. These trends confirm the strong link between the velocity flow field and HTC numerical results.

RAF Calculations

In this section the Reynolds analogy factor (RAF) has been calculated by the equation 3 for each diabatic simulation.

$$RAF = \frac{2St}{C_f} \tag{3}$$

The heat transfer coefficient is given by $St = \frac{\alpha}{v_\infty \rho_\infty c_\infty}$. Furthermore the skin friction coefficient is defined by $C_f = \frac{2\tau_w}{\rho_\infty v_\infty^2}$. For modelling the turbulent heat flux term $-\overline{u_j' T'}$ a constant turbulent Prandtl number $Pr_t = 0.9 \approx 1$ has been assumed. This assumption is a good approximation in simple flat plate boundary layer where thermal and momentum boundary layers evolve in the same way [25, 26, 27]. Furthermore for a typical flat plate layers the streamwise distribution of skin friction factor and heat transfer coefficient are known. It has been shown experimentally that [28] the ratio of skin friction and heat transfer does not significantly deviate from one. In a flow separation point in turn, the friction coefficient tends to zero, whereas the heat transfer does not necessarily decreases to zero. In such a situation the RAF will increase. In regions in which the Reynolds analogy factor significantly deviates from one no accurate prediction of the turbulent heat flux can be expected with a simple constant Prandtl

number. In regions in which RAF differs from one a more sophisticated turbulence model, describing the turbulent heat flux more accurate is required. Furthermore by visualising the RAF, regions of flow separation become visible. In figure 11 RAF calculations have been performed showing layouts focused on the top wall of the geometry for all turbulence models. In all calculations similar structures can be observed. The bulk part of the inlet channel shows RAF levels of one. Two oval lines of high level RAF occur which mark flow separating and reattaching the wall. The trailing edge channel can be roughly subdivided into two regions. Approximately one half shows RAF levels close to one (attached flow). The other half of the trailing edge channels exhibit RAF values ranging from one to 25. The highest RAF levels for all models are located along the inner sidewall where the separation occurs. The wide vortex leads the flow from the inner surface of the trailing edge duct to the core region of the channel. The counter-rotating vortices (Dean vortices) along the opposite sidewall brings the fluid towards the outer wall. Contrary to the vortex that produces the separation bubble along the inner wall, the Dean vortices do not generate a separation of the flow from the outer surface. In this region RAF values are maintained around 1. Here the Wilcox k-ω model predicts the largest RAF values, whereas the EARSM model predicts the greatest extend of the high-RAF region. High RAF levels are also concentrated along the corners in the bend region and on the inlet area. The lines observed along the leading edge of the geometry divide the duct into three parts. These lines are the footprint of the vortical structures observed in figure 8.

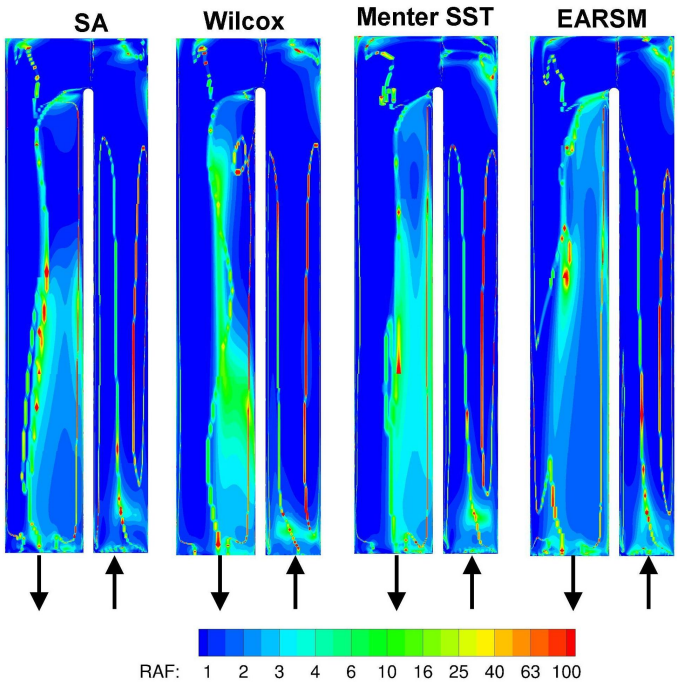

FIGURE 11. REYNOLDS ANALOGY FACTOR RAF

Conclusion

A turbine cooling channel geometry has been investigated with the TRACE code. The complex shape of the geometry provokes a flow field in which several vortices interact with each other. Such flow regimes are a challenging task for turbulence models. Four different turbulence models of different complexity have been used and results have been compared to PIV measurements made by Elfert [9]. The models Wilcox k-ω and EARSM reach more accurate velocity trends compared with experiments along the leading edge channel. Spalart Allmaras and EARSM show the most similar behavior to PIV data along the bend region of the trailing edge duct. Spalart Allmaras and EARSM are the turbulence models that present the nearest bubble lengths and size compared to experiments. SST shows the best agreement with PIV data concerning the secondary vortical structures, presenting along the inner sidewall the widest vortex compared to the other models. It could be confirmed that the highest order turbulence model, the EARSM model presents the most accurate overall velocity behaviour. Diabatic calculations have been performed in order to compare the turbulence modelling influence on wall heat transfer values. It has been shown that Stanton numbers generally increase with increasing turbulence model complexity. For the EARSM model the highest Stanton numbers were found. Furthermore the EARSM model leads to a major extension of the regions with higher heat transfer. Modelling of turbulent heat flux is based on the Reynolds analogy - a constant turbulent Prandtl number has been assumed. In the trailing edge channel, large regions of flow separation have been visualized. In these regions the turbulent heat flux cannot be modelled with a constant Prandtl number since thermal and momentum boundary layers evolve in a different way. A significant difference is expected between numerical predictions and experimental data. In this work the ability of current state-of-the-art RANS modelling is documented. Potential for further improvement lies in the application of full anisotropy resolving Reynolds stress transport models and higher order modelling of the turbulent heat flux.

ACKNOWLEDGMENT

The authors thank M. Elfert and E. Kügeler from DLR Institute of Propulsion Technology for fruitful discussions and helpful idea.

REFERENCES

[1] Han, J. , Dutta, S. : *Recent Developments in Turbine Blade Internal Cooling Annals of the New York Academy of Sci-*

ences Volume 934, HEAT TRANSFER IN GAS TURBINE SYSTEMS pages 162178, May 2001.

[2] Launder, B. E. , Iacovides, H. : *Internal blade cooling: The Cinderella of computational and experimental fluid dynamics research in gas turbines. Proceedings of the Institution of Mechanical Engineers* Part A: Journal of Power and Energy. 2007 April; 221(3): 265-290. eScholarID:1a9175 — DOI:10.1243/09576509JPE325.

[3] Weigand, B. , Semmler, K. , von Wolfersdorf, J. : *Heat Transfer Technology for Internal Passages of Air-Cooled Blades for Heavy-Duty Gas Turbines* Annals of the New York Academy of Sciences, Volume 934, HEAT TRANSFER IN GAS TURBINE SYSTEMS pages 179193, May 2001.

[4] Luo, J. , Razinsky, E. H. : *Analysis of Turbulent Flow in 180 deg Turning Ducts With and Without Guide Vanes* J. Turbomach. 131, 021011 (2009) (10 pages).

[5] Walker, D. , Zausner, J. : *RANS Evaluations of Internal Cooling Passage Geometries: Ribbed Passages and a 180 Degree Bend* Paper no. GT2007-27830 pp. 645-660 ASME Conf. Proc. / Year 2007 / Volume 4: Turbo Expo 2007.

[6] Schueler, M. , Dreher, H. M. , Neumann, S. O. , Weigand, B. , Elfert, M. : *Numerical Predictions of the Effect of Rotation on Fluid Flow and Heat Transfer in an Engine-Similar Two-Pass Internal Cooling Channel with Smooth and Ribbed Walls* DLR, Institute of Propulsion Technology, D-51170 Cologne, ASME J. Turbomachinery, Vol. 134 / 021021-1 2012.

[7] Lucci, J. M. , Amano, R. S. , Guntur, K. : *Turbulent Flow and Heat Transfer in Variable Geometry U-Bend Blade Cooling Passage* Paper no. GT2007-27120 pp. 159-167 ASME Turbo Expo 2007: Power for Land, Sea, and Air (GT2007) May 1417, 2007 , Montreal, Canada.

[8] Hellsten, A. : *New Advanced k-omega Turbulence Model for High-Lift Aerodynamics* AIAA Journal, Vol. 43, No. 9, 2005, pp. 1857-1869.

[9] Jarius, M. P. , Elfert, M. : *Flow investigation in a two-pass coolant channel with/without ribbed walls* DLR, Institute of Propulsion Technology, D-51170 Cologne, Proc 16th Intl Symp on Air Breathing Engines, Cleveland (OH), USA 2003.

[10] Franke, M.: *Turbulenzmodellierung in TRACE* DLR, Institut für Antriebstechnik, Numerische Methoden, Cologne

[11] Nürnberger, D. : *Implizite Zeitintegration für die Simulation von Turbomaschinenströmungen* PhD Thesis, Ruhr-Universität Bochum, September 2004, also DLR-FB 2004-27, 2004

[12] Spalart, P. R. , Allmaras, S. R. : *A One-Equation Turbulence Model for Aerodynamc Flows* AIAA Paper 92-0439, 1992.

[13] WILCOX, D. C.: *Turbulence Modeling for CFD* 2nd edition, DCW Industries, Inc., La Canada, California 91011, ISBN 0-9636051-0-0 November 1994

[14] Menter, F. R. , Kuntz, M. , Langtry, R. : Ten Years of Industrial Experience with the SST Turbulence Model. In *Turbulence, Heat and Mass Transfer 4*, ed: K. Hanjalic, Y. Nagano, and M. Tummers, Begell House, Inc., 2003, pp. 625 - 632.

[15] Schroll, M., Lange, L., Elfert, M : *Investigation of the effect of rotation on the flow in a two-pass cooling system with smooth and ribbed walls using PIV* Proceedings of ASME Turbo Expo, June 6-10, 2011, Vancouver, Canada, Paper GT-2011-46427.

[16] Elfert, M., Schroll, M., Förster, W. : *PIV-Measurement of secondary flow in a rotating two-pass cooling system with an improved sequencer technique* Proceedings of ASME Turbo Expo, June 14-18, 2010, Glasgow, UK, Paper GT-2010-23510.

[17] Adrian, R.J. : *Particle-Imaging Techniques for Experimental Fluid Mechanics* Annual Review of Fluid Mechanics, vol. 23, 1991.

[18] Raffel, M., Willert, C., Wereley, S., Kompenhans, J. : *Particle Image Velocimetry A practical guide (2nd Edition)* Springer Berlin Heidelberg, 448 pages (ISBN: 978-3-540-72307-3), 2007.

[19] Elfert, M., Jarius, M. P. : *Steady Fluid Flow Investigation using L2F and PIV in a Multi-Pass Coolant Channel* 9th Int. Symp. on Transport Phenomena and Dynamics of Rotating Machinery (ISROMAC-9), Honolulu, Hawaii, Feb.10-14, 2002.

[20] Westerweel J. : *Theoretical analysis of the measurement precision in particle image velocimetry* Exp Fluids 29: Suppl. S3-S12, 2002.

[21] Dreher, H. M. : *Numerical Prediction of Fluid Flow and Heat Transfer in a Two-Pass Internal Cooling Channel under Rotation* DLR, Institute of Propulsion Technology, IB-325-18-09, Cologne, University of Stuttgart ITLR 2009.

[22] Al-Qahtani, M. , Jang, Y. , Chen, H. , Han, J. : *Flow and heat transfer in rotating two-pass rectangular channels ($AR = 2$) by Reynolds stress turbulence model*. International Journal of Heat and Mass Transfer 45 (2002) 1823-1838

[23] Al-Qahtani, M. , Chen, H. , Han, J. : *A numerical study of flow and heat transfer in rotating rectangular channels ($AR = 4$) with 45° rib turbulators by Reynolds stress turbulence model*. Proceedings of ASME TURBO EXPO 2002, June 3-6, 2002, Amsterdam, The Netherlands

[24] Mochizuki, S. , Murta, A. , Shibata, R. , Yang, W. : *Detailed measurements of local heat transfer coefficients in turbulent flow through smooth and rib-roughened serpentine passages with a 180° sharp bend*. International Journal of Heat and Mass Transfer 42 (1999) 1925-1934

[25] Shankar Subramanian R. : *Heat Transfer in Flow Through Conduits*. Department of Chemical and Biomolecular Engineering, Clarkson University

[26] Schultz, B. H. : *On the application of Reynolds' analogy and the heat-exchange factor to the design of heat exchangers I*. Appl. sci. Res., Vol. A1

[27] Kays, W. M. , Crawford, M. E. : *Convective Heat and Mass Transfer*. 3rd Edition, 1993.

[28] Blair, M. F. : Influence of Free-Stream Turbulence on Turbulent Boundary Layer Heat Transfer and Mean Profile Development. In *Trans. ASME: J. Heat Transfer*, 105,pp. 33-40, 41-47, (1983).